AGU PUBLICATIONS

Journal of Advances in Modeling Earth Systems

RESEARCH ARTICLE

10.1002/2015MS000488

Mean-state acceleration of cloud-resolving models and large eddy simulations

C. R. Jones[1], C. S. Bretherton[1], and M. S. Pritchard[2]

[1]Department of Atmospheric Sciences, University of Washington, Seattle, Washington, USA, [2]Department of Earth System Science, University of California, Irvine, California, USA

Key Points:
- We introduce an acceleration technique for CRMs, LES, and superparameterized GCMs
- We achieve substantial speedup (2–16X) with little impact on cloud condensate for a range of cases
- We present applications to superparameterization and LES cloud-climate feedback studies

Correspondence to:
C. R. Jones,
crj6@uw.edu

Citation:
Jones, C. R., C. S. Bretherton, and M. S. Pritchard (2015), Mean-state acceleration of cloud-resolving models and large eddy simulations, *J. Adv. Model. Earth Syst.*, *7*, 1643–1660, doi:10.1002/2015MS000488.

Received 28 MAY 2015
Accepted 9 OCT 2015
Accepted article online 15 OCT 2015
Published online 29 OCT 2015

Abstract Large eddy simulations and cloud-resolving models (CRMs) are routinely used to simulate boundary layer and deep convective cloud processes, aid in the development of moist physical parameterization for global models, study cloud-climate feedbacks and cloud-aerosol interaction, and as the heart of superparameterized climate models. These models are computationally demanding, placing practical constraints on their use in these applications, especially for long, climate-relevant simulations. In many situations, the horizontal-mean atmospheric structure evolves slowly compared to the turnover time of the most energetic turbulent eddies. We develop a simple scheme to reduce this time scale separation to accelerate the evolution of the mean state. Using this approach we are able to accelerate the model evolution by a factor of 2–16 or more in idealized stratocumulus, shallow and deep cumulus convection without substantial loss of accuracy in simulating mean cloud statistics and their sensitivity to climate change perturbations. As a culminating test, we apply this technique to accelerate the embedded CRMs in the Superparameterized Community Atmosphere Model by a factor of 2, thereby showing that the method is robust and stable to realistic perturbations across spatial and temporal scales typical in a GCM.

1. Introduction

Accurately simulating moist convective processes is critical to representing atmospheric motions from local to global scales. The difficulty of realistically representing cloud and convective processes is exacerbated by the wide range of spatial and temporal scales that come into play [*Stevens and Lenschow*, 2001], with increased spatial resolution going hand-in-hand with increased computational cost.

Turbulence-resolving large eddy simulations (LESs) with grid spacings of 100 m or less are the highest resolution models typically used for probing the interplay among turbulence, clouds, and large-scale conditions. LES studies are generally limited to localized or short duration simulations due to the computational cost of high spatial resolution and the associated short time steps forced by Courant-Friedrichs-Lewy (CFL) stability considerations.

Cloud-resolving models (CRMs), similar to LES but with horizontal grid spacings of up to a few kilometers that do not fully resolve boundary layer eddies but do resolve the larger updrafts in cumulonimbus cloud systems, are skillful at simulating deep convection. They are typically used in regional domains up to 1000 km on a side, but pioneering global CRM simulations have been performed [*Tomita et al.*, 2005; *Miyamoto et al.*, 2013]. Superparameterization [*Grabowski*, 2001; *Khairoutdinov and Randall*, 2001], in which the cloud physics and moist convection parameterizations in a general circulation model (GCM) are replaced by an embedded 2-D CRM, is an approach to circumventing the limitations of cloud parameterizations in global models that has shown to be skillful in representing cloud and convection-related structures such as the Madden-Julian Oscillation [*Khairoutdinov and Randall*, 2001].

A practical challenge common to LES, CRMs, and superparameterized GCMs is the high computational cost imposed by the range of spatial and temporal scales being modeled. At the heart of this is the fact that resolving motion across scales is limited by the smallest spatial and shortest time scales. In cases exhibiting some degree of scale separation, one approach to reducing the computational cost is to artificially modify the governing equations of motion to reduce the separation between fast and slow time scales without adversely affecting the fidelity of the simulation.

In one of the earliest applications of modified physics to fluid modeling, *Chorin* [1967] introduced an artificial compressibility parameter into the equations of motion for an incompressible viscous fluid, yielding better numerical convergence properties but the same steady state solution. In the context of global ocean modeling, *Bryan* [1984] used a modified physics technique to reduce the separation between the slowly evolving deep ocean and the faster evolution of the upper ocean, again allowing shorter integration times without affecting the equilibrium solutions. *Liu et al*. [2004] rescaled the time variable for a subset of model levels in a coupled ocean-atmosphere GCM to achieve a similar goal of artificially enhancing the rate of deep ocean evolution relative to the atmosphere and shallow ocean layers. In this approach, dubbed "coordinated acceleration," the time gain is more modest than that obtained by *Bryan* [1984], but it also applies to nonequilibrium simulations and is easy to implement.

Kuang et al. [2005] developed an acceleration technique for atmospheric modeling. They reduced the scale between convective and large-scale dynamic motions in a global CRM by accelerating all diabatic processes while simultaneously reducing the Earth's radius and increasing its rotation rate. This rescaling is formally equivalent to a rescaling of the z coordinate [*Pauluis et al*., 2006]. Although this rescaling does effectively reduce the computation time, *Pauluis et al*. [2006] showed that the cloud ice and vertical velocity distributions were better represented with a coarser resolution unperturbed CRM that requires similar computational effort.

Xing et al. [2009] and *Slawinska et al*. [2015] detail a "sparse space and time" (SST) acceleration approach to speeding up the evaluation of the embedded CRMs in a superparameterized (SP) GCM (i.e., SSTSP). The sparse-space component reduces the effective horizontal extent that is used to calculate the convective scale forcing from the CRM on the GCM. This is similar in spirit to *Pritchard et al*. [2014], in which aspects of tropical convectively coupled dynamics were found to be resilient to CRM domain extent reduction in SP simulations. The sparse-time component reduces the evaluation time while increasing the large-scale forcing terms to fully account for the action of the large-scale forcing, in essence distorting the physics to accelerate the time evolution.

Although the acceleration strategy differs somewhat between each of these approaches, the goal is the same: to improve the computational efficiency by reducing the time scale separation between those motions that are computationally limiting and the slower scale motions. In this paper, we exploit the time scale separation between the evolution of horizontal-mean quantities and the turbulent fluctuations to develop a technique to speed up LES and CRM simulations by accelerating the mean-state tendencies of nonprecipitating moisture, temperature, and horizontal velocity.

We use a range of test cases to demonstrate this approach provides substantial computational speedups of a factor of 2–16 or more, depending on the case, with little impact on accuracy, including for the cloud condensate distribution, which is significantly distorted by other acceleration methods. As a culminating test, we apply this approach to accelerate the embedded CRMs in the Superparameterized Community Atmosphere Model (SPCAM) by a factor of 2, showing in the process that the method is robust and stable to realistic perturbations across spatial and temporal scales typical in a GCM.

We present our mean-state acceleration approach in section 2. We detail its implementation in the System for Atmospheric Modeling (SAM) LES in section 3. Case studies are presented in section 4. Simulation results are presented in sections 5 and 6. The relationship among the method's accuracy, stability, and the underlying time scales is briefly explored in section 7. Concluding remarks are presented in section 8.

2. Mean-State Acceleration Scheme

In this section, we develop the mean-state acceleration technique. An alternate motivation using the seamless heterogeneous multiscale formalism [*Abdulle et al*., 2012] is presented in Appendix A.

Consider a scalar field $\phi(\mathbf{x}, t)$ that evolves according to

$$\frac{\partial \phi}{\partial t} = f(\phi, t), \tag{1}$$

where f is a specified evolution equation, $\mathbf{x} = (x, y, z)$ are the space coordinates, and t is time. To clarify our notation, ϕ and t are interpreted as independent variables on the right-hand side of (1), with the t argument representing only the explicit time dependence of f, such as through externally applied large-scale forcings.

A realistic evolution equation for ϕ is coupled to the circulation and other internal state variables which are coevolving. We will explicitly account for this after motivating mean-state acceleration in terms of a single scalar field, but for the time being consider this coupling to be implicit in (1).

Expanding $\phi(\mathbf{x},t)=\bar{\phi}(z,t)+\phi'(\mathbf{x},t)$, where the overline denotes the horizontal-mean state and the prime denotes fluctuations about the mean, we can decompose (1) into the system

$$\frac{\partial\bar{\phi}}{\partial t}=\bar{f}(\bar{\phi},\phi',t), \tag{2}$$

$$\frac{\partial\phi'}{\partial t}=f'(\bar{\phi},\phi'). \tag{3}$$

For atmospheric fields such as temperature *T*, humidity *q*, and horizontal winds in a domain wide enough to encompass multiple turbulent eddies but small enough to have horizontally homogeneous turbulent statistics, the horizontal-mean state typically evolves slowly compared to the turbulent fluctuations. There is no fundamental reason for this time scale separation, so it must be assessed on a case-by-case basis. However, since the mean state evolves as a result of all eddies, not just the most vigorous, some time scale separation is to be expected. In this case, we can regard the eddy statistics as being "tethered" to (i.e., approximately determined by) the current mean state and the external forcings.

The strongest eddy motions limit the time step for advancing the turbulent fluctuations. The motivating idea for mean-state acceleration is to artificially accelerate the slow rate of horizontal-mean-state evolution by an "acceleration factor" without directly affecting the turbulent eddies, or equivalently, artificially slowing down the eddy evolution compared to that of the mean state.

Formally, we accomplish this by rescaling (2) under the assumption that $\bar{\phi}$ evolves on a long characteristic time scale that is $a>1$ times as long as the time scale of eddy evolution. We introduce a "slow" time variable $\tau=t/a$. Applying the chain rule to rewrite (2) in terms of τ yields

$$\frac{\partial\overline{\phi_a}}{\partial\tau}=a\bar{f}(\overline{\phi_a},\phi',a\tau), \tag{2'}$$

where the subscript *a* denotes that this variable is accelerated. Treating τ as a dummy variable and reassigning $\tau\rightarrow t$, we recombine (2′) with (3) to yield a new accelerated evolution equation for $\phi_a=\overline{\phi_a}+\phi'$,

$$\frac{\partial\phi_a}{\partial t}=f(\phi_a,at)+(a-1)\bar{f}(\phi_a,at), \tag{4}$$

where for notational convenience we have recombined the $\bar{\phi}_a$ and ϕ' arguments into ϕ_a, with $\bar{f}(\phi_a,at)=\bar{f}(\bar{\phi}_a,\phi',at)$ and $f(\phi_a,at)=\bar{f}(\phi_a,at)+f'(\bar{\phi}_a,\phi')$. The horizontal means of ϕ_a and the unaccelerated ϕ are related by

$$\overline{\phi_a(\mathbf{x},t)}\approx\overline{\phi(\mathbf{x},at)}. \tag{5}$$

Equation (4) effectively amounts to evolving the mean state at a rate that is *a* times faster than the perturbations. Comparing (1) with (4), we see that this acceleration approach takes the form of an additional large-scale mean-state acceleration tendency on the right-hand side of (1). This has the benefit of being simple to implement within an existing CRM framework and requires no a priori knowledge of the form of *f* aside from the assumed time scale separation.

Having motivated the mean-state acceleration approach in terms of a single scalar field, we now generalize it to multiple accelerated fields. Consider a CRM consisting of variables exhibiting scale separation that may be accelerated, $\Phi=(\phi_1,\phi_2,\ldots,\phi_n)$, as well as fast-evolving variables that are not subject to acceleration, $\Psi=(\psi_1,\ldots,\psi_N)$. Given specified tendencies $\mathbf{f}[\Phi,\Psi]$ and $\mathbf{g}[\Phi,\Psi]$ such that

$$\frac{\partial\Phi}{\partial t}=\mathbf{f}[\Phi,\Psi](\mathbf{x},t)$$

$$\frac{\partial\Psi}{\partial t}=\mathbf{g}[\Phi,\Psi](\mathbf{x},t),$$

the analogue to (4) is

$$\frac{\partial \Phi_a}{\partial t} = \mathbf{f}[\Phi_a, \Psi](\mathbf{x}, at) + (a-1)\bar{\mathbf{f}}[\Phi_a, \Psi](z, at), \tag{6}$$

$$\frac{\partial \Psi}{\partial t} = \mathbf{g}[\Phi_a, \Psi](\mathbf{x}, at). \tag{7}$$

As in the case of a single scalar, in order for Φ to be a candidate for acceleration by this technique, we require that the horizontal mean, $\bar{\Phi}(z,t)$, evolves with a characteristic time scale much slower than that of the turbulent eddies. More to the point, we require that $\bar{\Phi}$ evolves slowly enough that there exists an a for which the rescaling in (6) still maintains scale separation (albeit a reduced one) for each $\overline{\phi_j}$ relative to ϕ'_j.

In essence, our approach is simply to force Φ' and Ψ to respond to the slow changes in $\bar{\Phi}$ at a more rapid rate than they otherwise would. Since this approximation relies on time scale separation for its validity, a must be chosen small enough that Φ' and Ψ remained tethered to $\bar{\Phi}$. This also constrains the variables Ψ that we can afford not to accelerate. Any variable ψ for which the mean storage term $\partial\bar{\psi}/\partial t$ is small on long time scales can safely remain unaccelerated. Conversely, if $\partial\bar{\psi}/\partial t$ is nonnegligible on long time scales, it will contribute to the mean-state tendency, and ψ must be accelerated.

2.1. Desirable Features of Mean-State Acceleration

The proposed mean-state acceleration scheme has several advantages which we highlight here.

Ease of implementation. It is formulated simply as an additional horizontally uniform forcing tendency that is easy to calculate as a horizontal average of information already calculated in each time step, so implementation is straightforward.

Versatility. Mean-state acceleration can be applied to a model operating as a standalone LES or CRM, or to an embedded CRM in a superparameterized model. We present examples for all three of these configurations in the remainder of this paper.

Steady state convergence. Consider a model that is currently in statistical steady state. By definition, the net mean horizontal tendency of each variable is zero, and so applying the acceleration technique does not alter the steady state behavior. Thus, mean-state acceleration is especially well suited for steady state sensitivity studies. By contrast, approaches which accelerate only the large-scale forcing term or some other subset of terms risk perturbing the steady state equilibrium relative to an unaccelerated simulation.

The unaccelerated limit. Mean-state acceleration gracefully transitions between accelerated and unaccelerated operation. Choosing $a = 1$ in (6) recovers the original system exactly, and in principle a can be varied during the course of a simulation to meet accuracy or stability needs.

Minimal cloud bias. This approach accelerates the net mean tendency of Φ, rather than accelerating only a subset of the processes contributing to this tendency. This allows all relevant physical processes to be accounted for in the horizontal mean. Because the statistics of the Ψ variables (such as precipitating water mixing ratio) and the horizontal variability of the Φ' variables (such as turbulent velocity variances) are tethered to the $\bar{\Phi}$ variables, they also have minimal sensitivity to increased acceleration, as verified in section 5.

The robustness of predicted cloud fields (e.g., cloud water content) and turbulence statistics to increased acceleration is an important advantage compared to other acceleration approaches. For instance, unsatisfying aspects of both DARE and the SSTSP acceleration approach include large sensitivity of the cloud fields to the acceleration parameter. *Pauluis et al*. [2006, Figure 4] shows that the peak of the cloud ice fraction distribution shifts downward with increasing acceleration factor, and the shape of the distribution itself is increasingly distorted in radiative-convective equilibrium simulations. *Slawinska et al*. [2015, Figure 7] shows that temporal acceleration overestimates the mean cloud condensate in the SSTSP simulations, and that this overestimation scales nearly linearly with the acceleration factor. For example, with a temporal-acceleration factor of 4, the cloud water content is as much as 2–3 times greater than that of the nonaccelerated simulation through the full vertical extent of the domain. *Slawinska et al*. [2015] implicated the lack of acceleration of the CRM cloud microphysical tendency as contributing to this mean bias.

3. Detailed Implementation

In this section, we detail the implementation of the mean-state acceleration technique in version 6.7 of the System for Atmospheric Modeling (SAM) [*Khairoutdinov and Randall*, 2003], supplied and maintained by Marat Khairoutdinov of Stony Brook University. The advection scheme of *Blossey and Durran* [2008] is used for the three advected scalars, liquid/ice water static energy $s_\ell = c_p T + gz - L_v(q_c + q_r) - L_s(q_i + q_s + q_g)$, total nonprecipitating water mixing ratio $q_t = q_v + q_c + q_i$, and precipitating water mixing ratio $q_p = q_r + q_s + q_g$. Here the mixing ratios refer to water vapor (q_v), cloud condensate (q_c), ice condensate (q_i), rain (q_r), snow (q_s), and graupel (q_g). As noted by *Blossey et al*. [2013], this model version produces less numerical diffusion than the default SAM at the sharp, poorly resolved inversion that caps stratocumulus cloud layers, resulting in higher and more realistic simulated stratocumulus liquid water paths. The cloud liquid water and temperature are diagnosed from the advected scalars using the assumption of exact grid-scale saturation in cloudy grid cells. The *Khairoutdinov and Kogan* [2000] scheme is used for conversion between cloud and rain water.

We apply mean-state acceleration throughout the full duration of the simulation, including during the model spin-up phase. In our configuration of SAM, the natural prognostic variables for acceleration are horizontal momentum (u, v), q_t, and s_ℓ. In all cases considered, periodic lateral boundary conditions are used, so $\bar{w} = 0$ within the CRM, so w is trivially accelerated. The effects of any externally specified mean vertical velocity on other variables are included through the large-scale forcing. Although we accelerate u and v in all simulations presented here, little would be lost by neglecting to accelerate the momentum variables when large-scale velocity nudging is being applied, since in that case our acceleration technique effectively reduces to nudging u and v with a different time scale.

We do not accelerate the precipitation mixing ratio q_p. On philosophical grounds, this is because there is no long-term storage term of q_p. On practical grounds, naively accelerating q_p can violate the model CFL stability condition when the fall speed of precipitation becomes significant.

Mean-state acceleration is applied as an additional large-scale tendency after all other physical and dynamic processes have been applied and is implemented as an explicit forward Euler term. Specifically, if a single unaccelerated step of the CRM evolves the state from time t to time $t + \Delta t$, then acceleration is applied at the end of the time step as

$$\phi(t + a\Delta t) = \phi(t + \Delta t) + (a - 1)\left(\overline{\phi(t + \Delta t)} - \overline{\phi(t)}\right) \qquad \text{for } \phi \in \{s_\ell, q_t, u, v\}, \tag{8}$$

$$\psi(t + a\Delta t) = \psi(t + \Delta t) \qquad \text{for } \psi \in \{q_p\}. \tag{9}$$

Note here that we have explicitly included the time acceleration in the time variable, which allows for direct comparison across simulations run with different acceleration factors.

To assure positivity of q_t, in any grid cell for which the acceleration tendency would drive $q_t(x, y, z)$ negative, we account for the negative excess and then set $q_t(x, y, z) = 0$. We then make a second pass, distributing the negative excess proportional to q_t in the remaining grid cells. That is, if the mean remaining q_t that needs to be removed from level z is $-\overline{\delta q_t}$, then

$$q_t(x, y, z) = q_t(x, y, z)\left(1 - \frac{\overline{\delta q_t}(z)}{\overline{q_t}(z)}\right). \tag{10}$$

We find this situation only arises in cases of deep convection.

4. Case Studies

As a proof of concept for this acceleration approach, we apply it to a series of case studies that have previously been the subject of LES modeling studies. Several are drawn from Global Water and Energy Experiment (GEWEX) Cloud System Studies (GCSS) intercomparison studies.

4.1. BOMEX

To test the acceleration scheme under shallow convection, we use a nonprecipitating, quasi-steady marine shallow cumulus case derived from the Barbados Oceanographic and Meteorological Experiment (BOMEX)

[*Holland and Rasmusson*, 1793]. We follow the GCSS intercomparison specifications presented in *Siebesma et al*. [2003]. Precipitation is turned off, and radiative cooling is accounted for in the specified large-scale forcings for this case.

4.2. DYCOMSII-RF01

The first research flight of the Second Dynamics and Chemistry and Marine Stratocumulus Experiment (DYCOMSII-RF01) observed a nocturnal nondrizzling stratocumulus-capped mixed layer [*Stevens et al*., 2003], which was subsequently used as the basis for GCSS single column model and LES intercomparisons [*Zhu et al*., 2005; *Stevens et al*., 2005]. SAM simulations are based on the DYCOMSII-RF01 case setup documented in *Stevens et al*. [2005]. Precipitation is allowed for these simulations, and an idealized longwave radiative flux formulation is utilized. Subsidence is specified in terms of a constant divergence, and geostrophic forcing is used to drive the horizontal-mean velocities.

4.3. KWAJEX

For a more stringent test of the acceleration scheme, we perform CRM simulations of deep convection in a region over the central tropical Pacific Ocean during the Kwajalein Experiment (KWAJEX). The case setup generally follows that of the BIG simulation of *Blossey et al*. [2007], with salient details described here. Time-dependent SST and mean vertical velocity w_{ls} are prescribed, as are large-scale horizontal advection tendencies for s_ℓ and q_t. The mean horizontal velocity profiles are nudged to the observed, time-dependent velocity profiles on a 2 h time scale. Simulations were performed over a 50 day period of KWAJEX (0600 UTC 24 July 1999 to 0600 UTC 12 September 1999). The vertical grid uses 64 levels, with grid spacing that increases from 75 m at the surface, to an approximately uniform 400 m in the troposphere, to 1 km near the 27 km domain top. The horizontal grid has a 1 km by 1 km resolution with 256 levels in each direction. For consistency with *Blossey et al*. [2007], the default SAM one-moment microphysics is used.

4.4. CGILS S12

An overview of CGILS is provided by *Zhang et al*. [2013]. The goal of CGILS was to develop prototype cases for comparing the response of subtropical cloud-topped boundary layers to idealized climate perturbations in both single-column models and LES. Cases were set up for three different cloud regimes. In the present study, we focus only on the well-mixed stratocumulus regime, with forcings corresponding to typical summer conditions at the S12 location along a transect across the northeast Pacific Ocean extending from near San Francisco past Hawaii. We use this case to test the acceleration scheme's ability to reproduce the steady state sensitivity of the unaccelerated simulations to climate change inspired perturbed forcings. The LES is configured as described in *Bretherton et al*. [2013]. From *Blossey et al*. [2013] and *Bretherton et al*. [2013], we consider the time-independent, diurnally averaged control (CTL) simulation and P2 perturbation. The CTL simulation corresponds to July 2003, monthly mean boundary conditions and idealized advective forcings. The P2 simulation represents an idealized large-scale climate change nominally corresponding to a uniform 2K warming of the SST locally and over the entire tropics, along with a moist-adiabatic increase of the free tropospheric temperature profile that might accompany such an SST increase, and a moistening of the free troposphere to maintain constant relative humidity.

Radiation is calculated using the Rapid Radiative Transfer Model - GCM version scheme [*Mlawer et al*., 1997]. Both the horizontal winds and free troposphere temperature and humidity profiles are nudged to the specified mean state.

5. CRM and LES Simulation Results

In this section, we present simulation results for the cases described in the previous section. In what follows, CTL refers to an unaccelerated control simulation, and "Nx" refers to simulations with $a = N$. Time has been scaled in all cases to refer to the "accelerated time" at.

Throughout this section, we use the total condensed water path (TWP) as a metric to assess the accuracy of mean-state acceleration. For BOMEX, DYCOMSII-RF01, and the CGILS simulations, this is equivalent to the

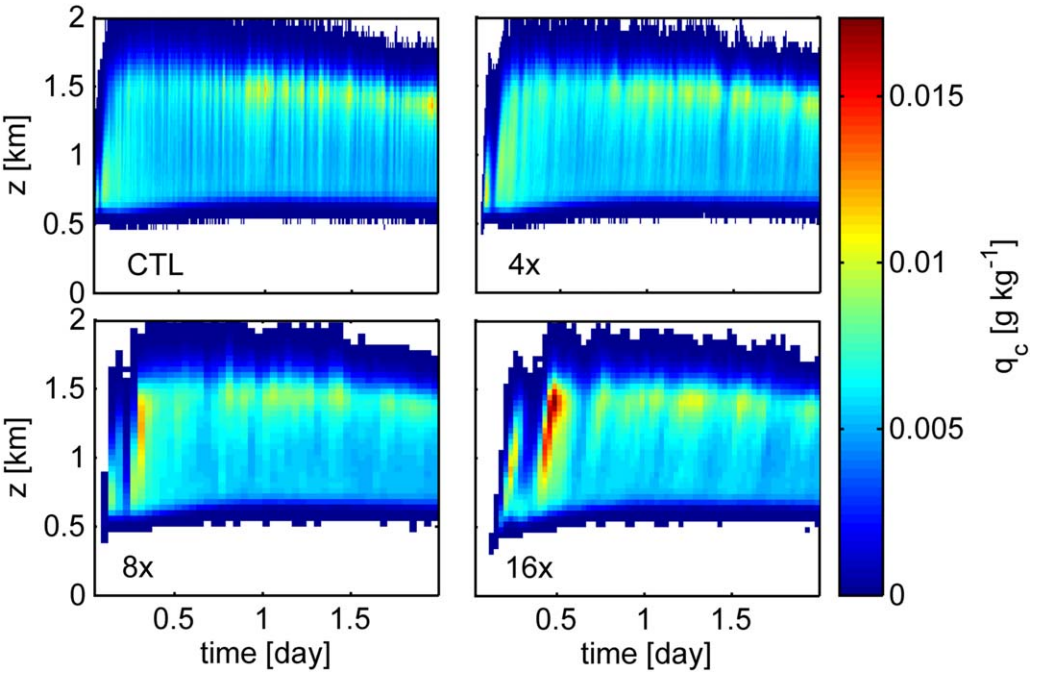

Figure 1. Time-height plots of q_c (in units of g kg^{-1}) for BOMEX simulations.

liquid water path (LWP). For each case, we present a figure of TWP extending across the full range of stable acceleration factors.

5.1. BOMEX

We begin with the BOMEX shallow cumulus case. Simulations remain stable for $a < 48$. Figure 1 shows time-height series of cloud water mixing ratio (q_c) for acceleration factors ranging from 1 to 16. The simulations evolve remarkably similarly, even for the largest acceleration factor.

Figure 2 shows time series of the shaded cloud fraction (CF) for $a \leq 16$ and TWP for $a \leq 40$. Both the TWP and CF time series demonstrate that the duration of the initial transient period increases with acceleration factor, indicating that mean-state acceleration does not decrease the computational time required for the model to "spin-up." This is to be expected because the turbulent eddies, which are not accelerated, require approximately the same number of time steps after initialization to equilibrate to the mean state.

The steady state mean and low frequency evolution after the initial transient period shows excellent agreement for the whole range of acceleration factors. The high-frequency variability lengthens somewhat with

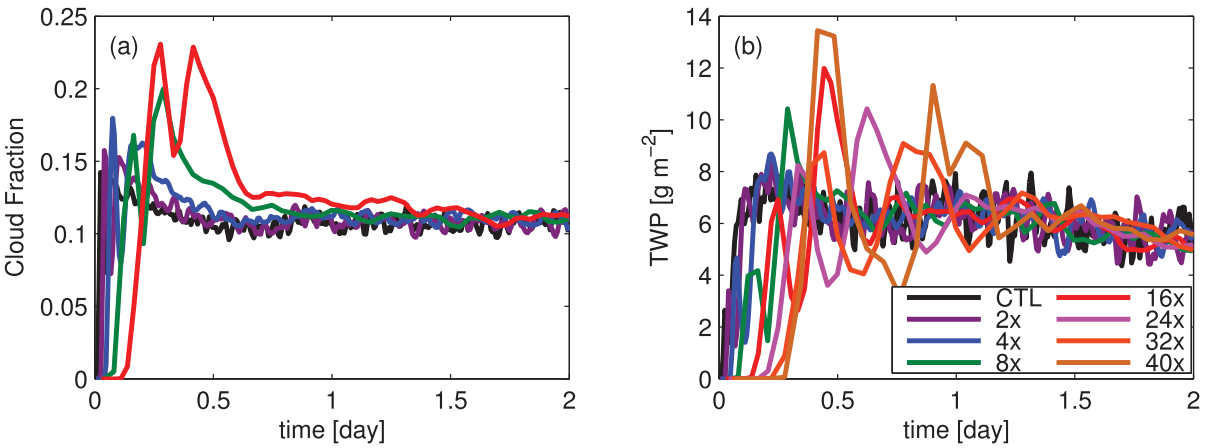

Figure 2. BOMEX time series of (a) vertically projected cloud fraction and (b) TWP.

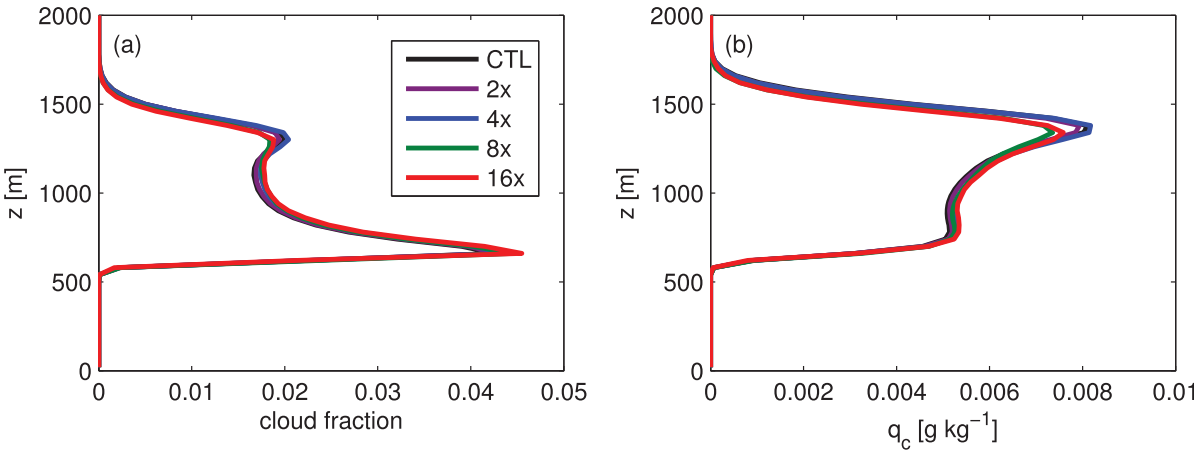

Figure 3. BOMEX 36–48 h mean profiles of (a) cloud fraction and (b) qc.

acceleration factor, and there is slight tendency for the variance to decrease with increased acceleration. For $a > 8$, the transient LWP and CF response becomes increasingly distorted, leading us to conclude that $a = 8$ is an approximate upper limit for accuracy. It is, however, quite impressive that integrated measures of mean cloud statistics agree so well even with a very large acceleration of the mean tendencies.

Figure 3 shows the vertical structure of q_c and cloud fraction averaged over the final 12 h of the simulation. Both show excellent agreement across acceleration factors up to 16. Although the q_c peak is slightly lower for $a \geq 8$, this result depends on the averaging window and is not systematic. This confirms the design goal that the acceleration factor does not affect the mean statistical steady state. That it works so well even for the 16X simulation is remarkable, since such a large acceleration factor runs the risk of violating the requirement that the turbulent eddies fully respond to changes in the mean state within a single model time step.

5.2. DYCOMSII-RF01

The boundary layer growth and cloud evolution in the DYCOMSII-RF01 case are strongly controlled by the simulated cloud top entrainment. Adequately capturing the effect of this inherently turbulent phenomenon provides another challenge to our method. Simulations are stable for $a < 40$. Figure 4 shows time-height series of cloud fraction for $a = 1$ to $a = 8$. Qualitatively, the whole range of acceleration factors captures the same evolution. A well-mixed stratocumulus deck deepens until the boundary layer decouples and it transitions to a decoupled, broken stratocumulus state.

Quantitative differences across acceleration factors are seen more clearly in the TWP time series of Figure 5. Up to 4X acceleration, the TWP evolution curves are nearly indistinguishable throughout the simulation. For 8X acceleration, the TWP is overestimated by nearly 10 g m^{-2} during the stratocumulus period, and the onset of stratocumulus breakup is delayed by several hours. This response is associated with the accelerated deepening of the boundary layer as a increases. We hypothesize that as the inversion rise rate is accelerated, this distorts the effect of eddies on the inversion structure. In particular, the eddies do not have time to fully adjust the inversion structure for large a, reducing the efficiency of entrainment and leading to a thicker cloud that persists somewhat longer. The ultimate decoupled steady state still agrees for all acceleration factors, but in order to efficiently and accurately capture the evolution of the well-mixed state, we find 4X to be the ideal acceleration factor.

5.3. KWAJEX

We next apply acceleration to the KWAJEX deep oceanic convection case. Acceleration factors larger than 6X were found to be unstable due to CFL violation. Figure 6 shows time-height series of horizontal-mean q_c and cloud ice, q_i, for CTL and 4X accelerated simulations. For clarity, we present only the first 10 days of the full 50 day simulation, which are representative of the overall behavior. Qualitatively, these fields evolve similarly in both CTL and 4X simulations, although there is a tendency for the q_i maxima to be larger in the 4X simulation.

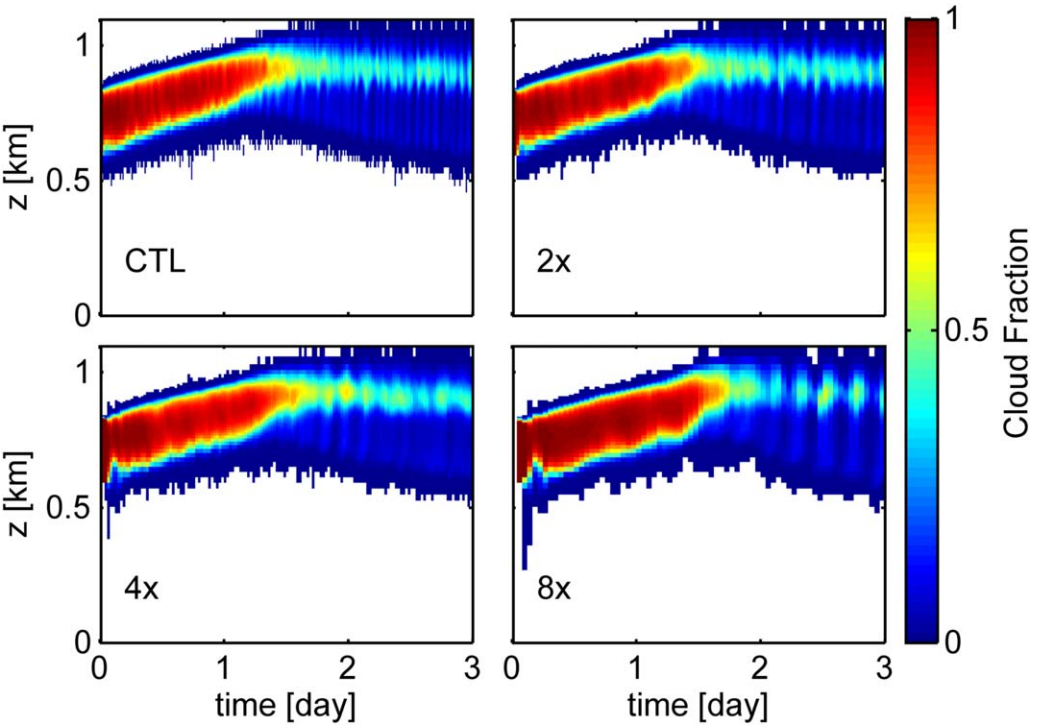

Figure 4. Time-height plots of cloud fraction for DYCOMSII-RF01 simulations.

Profiles of q_c and q_i averaged over the full 50 day period (Figure 7a) are nearly identical in the unaccelerated and accelerated simulations. The cloud fraction (Figure 7b) is systematically larger in the CTL case than the accelerated simulations above 12 km. This excess cloud is optically thin and radiatively negligible; the acceleration has no significant effect on the time-mean longwave and shortwave radiative heating profiles (not shown).

Cloud water path and surface precipitation are shown in Figure 8. Both the TWP and precipitation time series are in close agreement. The accelerated precipitation systematically lags behind that of the CTL simulation. The timing error in surface precipitation is a consequence of not accelerating the q_p mean state. Given identical rain droplets falling with the same terminal speed from the same level, the droplet will reach the surface in approximately the same number of time steps in both control and accelerated simulations. Thus, the dilation of time in the accelerated runs induces the delay. The total accumulation is not substantially affected by acceleration. For example, over the full 50 day simulation, total precipitation in CTL is 352 mm, compared to 350 mm for 4X.

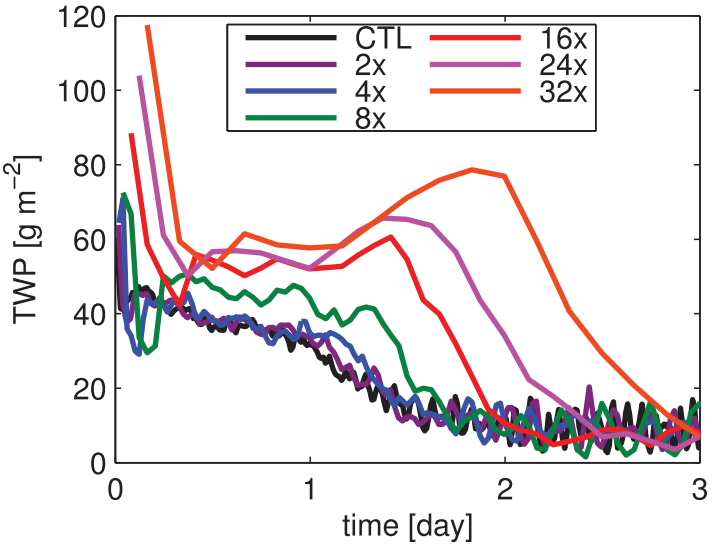

Figure 5. DYCOMSII-RF01 time series of TWP.

5.4. CGILS S12

Because a statistical steady state is unaffected by mean-state acceleration, this technique is ideal for cloud feedback sensitivity studies

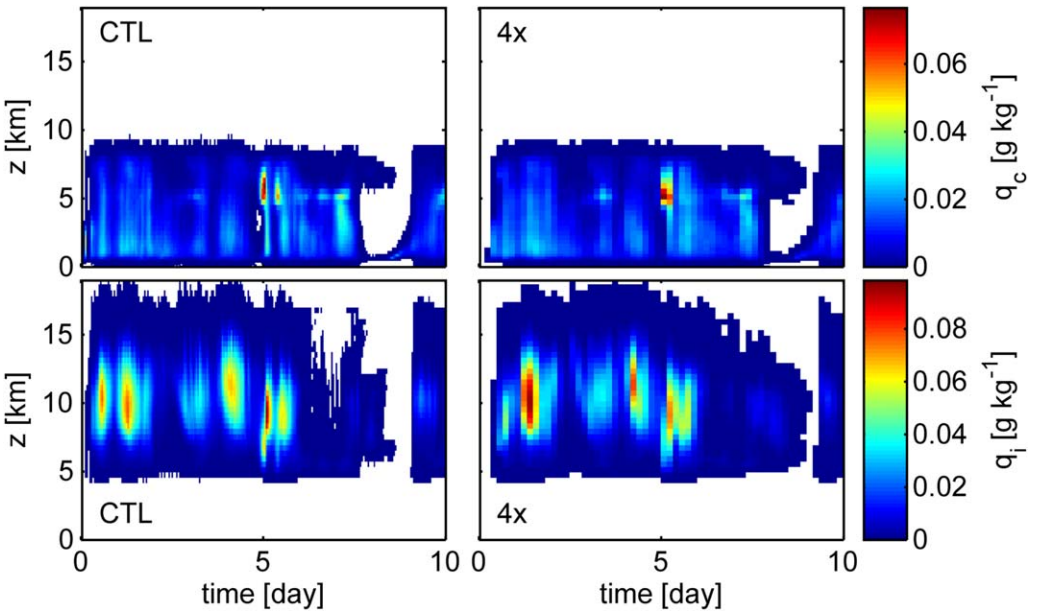

Figure 6. Time-height plots for the first 10 days of the KWAJEX case of (top) cloud liquid and (bottom) cloud ice for the (left) control and (right) 4X simulations.

such as CGILS [*Zhang et al.*, 2013]. Figure 9 shows time series of LWP and 8–10 day mean profiles of q_c for the CGILS S12 CTL and P2 simulations with up to 24X acceleration ($a = 32$ is unstable). The CTL and P2 simulations both feature a well-mixed stratocumulus deck with full cloud cover, so the LWP response is a good proxy for the radiative effect of the perturbation. The full extent of the LWP evolution of the LWP is remarkably well captured in the 8X and 24X simulations with a corresponding reduction in computational expense, although the spin-up time and transient variability increase with a. The steady state mean profiles verify that the vertical structure of the mean state is preserved under acceleration, even for 24X acceleration.

6. Accelerated SPCAM

In the previous section, we successfully applied mean-state acceleration to CRM simulations covering stratocumulus, shallow cumulus, and deep convection regimes. We now use this technique to accelerate a superparameterized model by applying it within the embedded CRMs of the Superparameterized Community

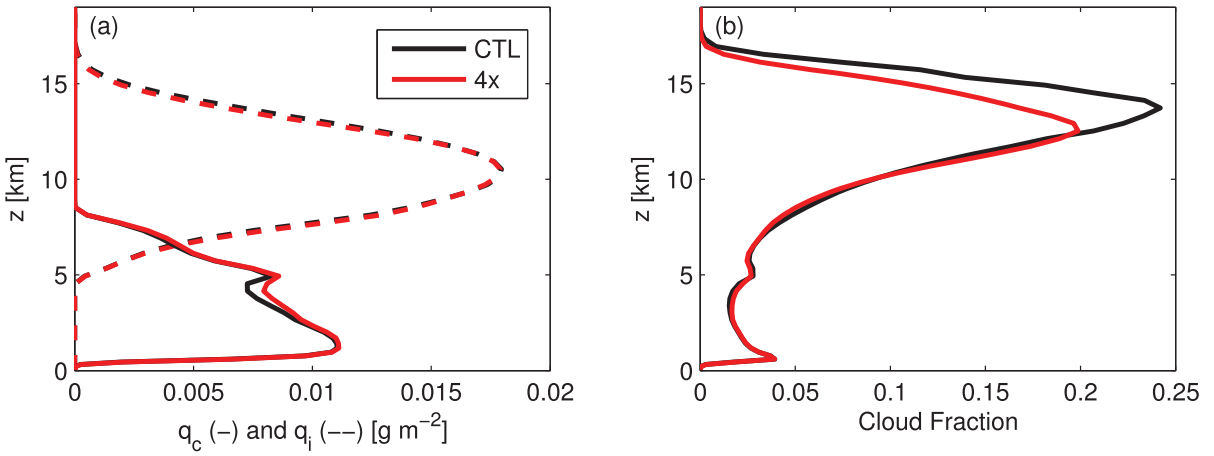

Figure 7. KWAJEX 50 day averaged profiles of (a) cloud water and ice profiles and (b) cloud fraction.

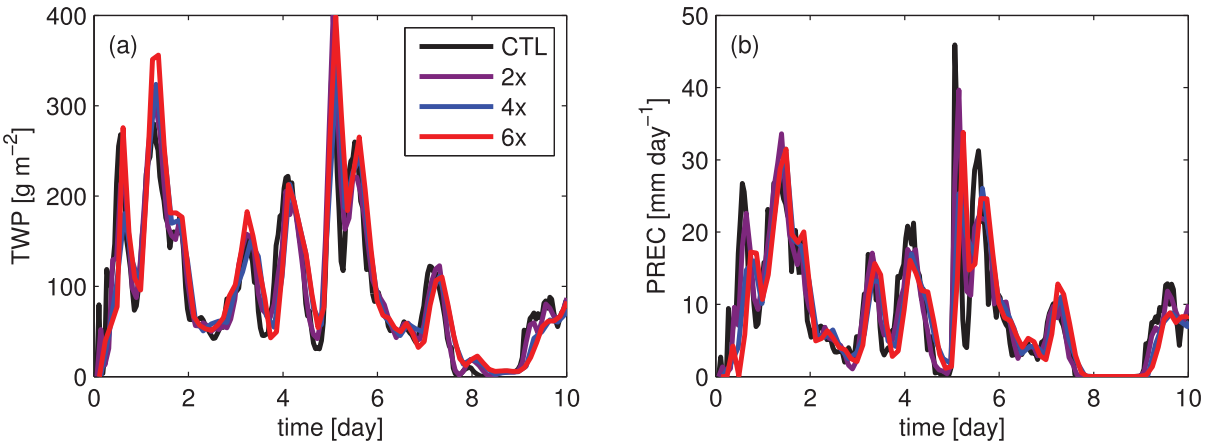

Figure 8. KWAJEX 10 day time series of (a) TWP and (b) surface preciptation.

Atmosphere Model v.3.0. (SPCAM) [*Khairoutdinov et al.*, 2005]. This is a stringent test of our technique, because the CRMs are subjected to realistic forcings acting across a wide range of spatial and temporal scales.

Our version of SPCAM uses a spectral dynamical core at T42 triangular truncation to represent global dynamics at a 30 min time step. An embedded cyclic 2-D CRM is run in each of its over 8000 host grid columns to replace traditional cloud and turbulence parameterizations. The CRM horizontal resolution is 4 km and its time step is 20 s. As in the earlier tests, simplified bulk one-moment microphysics are used.

As in our case studies, we accelerate s_ℓ and q_t, but not precipitation q_p. Bearing in mind the discussion in Appendix A, this choice is natural for SPCAM because the prognostic GCM-resolved thermodynamic variables are T and q, while q_p is a diagnosed quantity in CAM. We also choose not to accelerate the horizontal velocities because they are already nudged to the GCM-prognosed values. This should not adversely affect the results, though one could easily accelerate u and v if desired.

Unlike the implementation in SAM6.7, the pilot SPCAM implementation is not forced to conserve total water through the application of equation (10), though we will demonstrate it nonetheless performs very well.

The only change needed to the scale coupling that links SPCAM's embedded CRMs to their host GCM is to reduce the number of CRM integration steps taken between GCM time steps to conserve actual time under CRM mean-state acceleration. The actual time frequency of radiative transfer calculations is unchanged in this approach. We reiterate that a key difference compared to the SSTSP approach is that none of the GCM-scale provisional large-scale forcing tendencies transmitted from GCM to CRM need to be modified

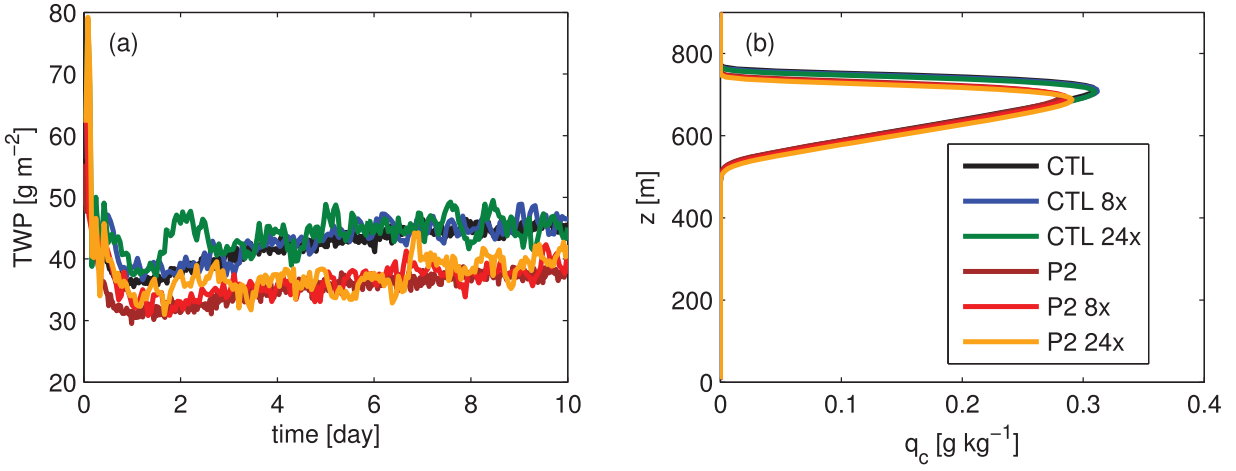

Figure 9. CGILS S12 (a) TWP time series and (b) 8–10 day mean profiles of cloud condensate.

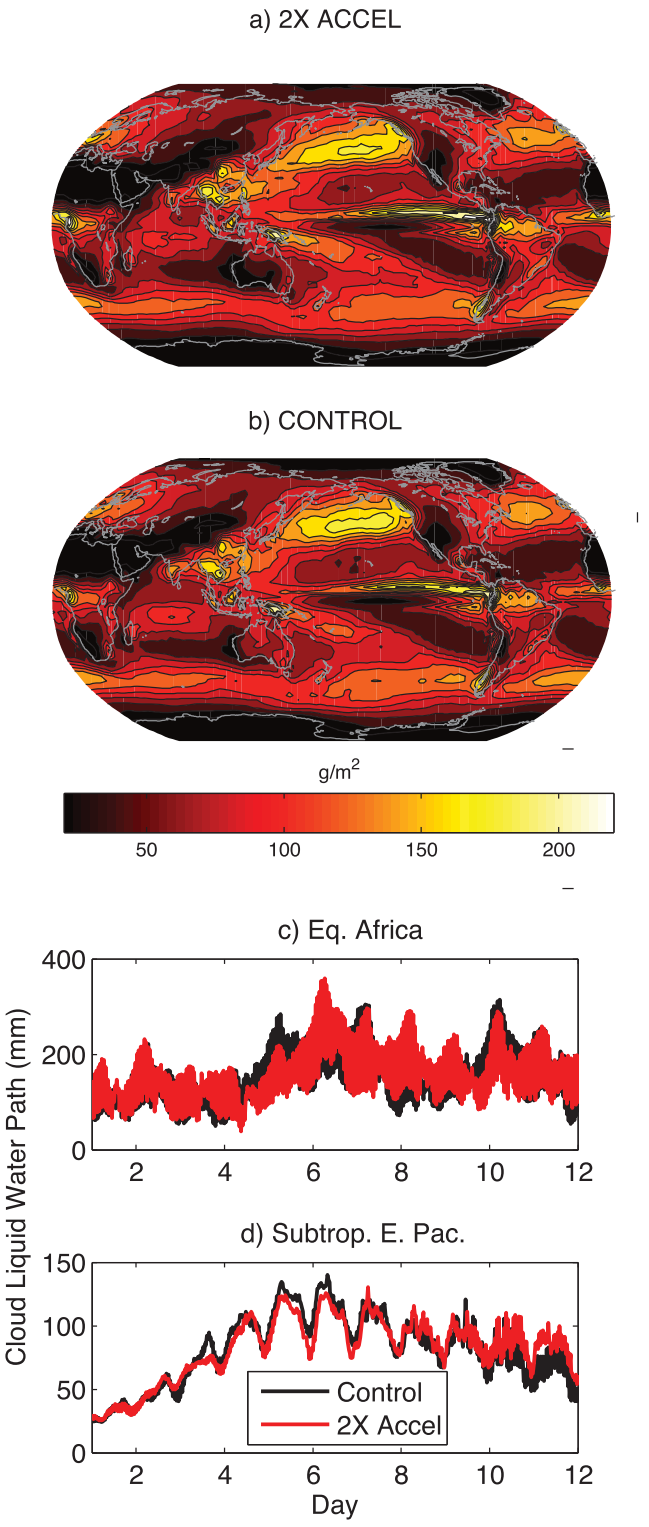

Figure 10. (top) SPCAM annual mean LWP climatology from 4 year simulations using standard 32-column CRMs under (a) 2X accelerated and (b) control configurations. (bottom) Time series of LWP in subregions (see text) from 12 day simulations using small eight-column CRMs.

under the acceleration approach such that modifying the number of CRM integration steps is the only change required for a SP implementation.

Two pairs of SPCAM simulations are performed, each with and without two-fold acceleration. The first is a pair of 4 year climatological simulations for the period 1981–1984 in which a configuration of SPCAM with a standard CRM extent of 32 columns (128 km extent) is used. The second is a pair of shorter 12 day simulations that are additionally accelerated by using a method of sparse-space SP by applying unusually small CRMs that are only eight columns (32 km) wide, i.e., the "micro-CRM" approach in *Pritchard et al.* [2014], which demonstrates that stacking these techniques can achieve eightfold SPCAM acceleration—a factor of four from the domain extent reduction, and an additional factor of two from CRM time acceleration.

Figure 10 (top) show the 4 year mean cloud LWP has a very similar geographical distribution in the standard-CRM SPCAM control and 2X acceleration simulations. The bottom figures show time series of LWP averaged over equatorial Africa (10°S–10°N,10°E–30°E) and the subtropical Northeast Pacific (20°N–35°N, 140°W–110°W) for the two micro-CRM SPCAM simulations, each with the same initial GCM-scale state. Especially at early lead times, the control and 2X acceleration experiments evolve nearly identically before diverging in detail due to the inevitable growth of small perturbations between them, after which only a statistical comparison is meaningful. In both regions, the 2X simulation reproduces a similar evolution on the multiday time scale, a similar diurnal cycle, and a similar degree of high-frequency variability. This demonstrates that the regional statistics of cloud water content are reasonably insensitive to mean-state acceleration.

Figure 11 demonstrates the same for the mean surface precipitation rate. The mean precipitation patterns (top) show good agreement, and the

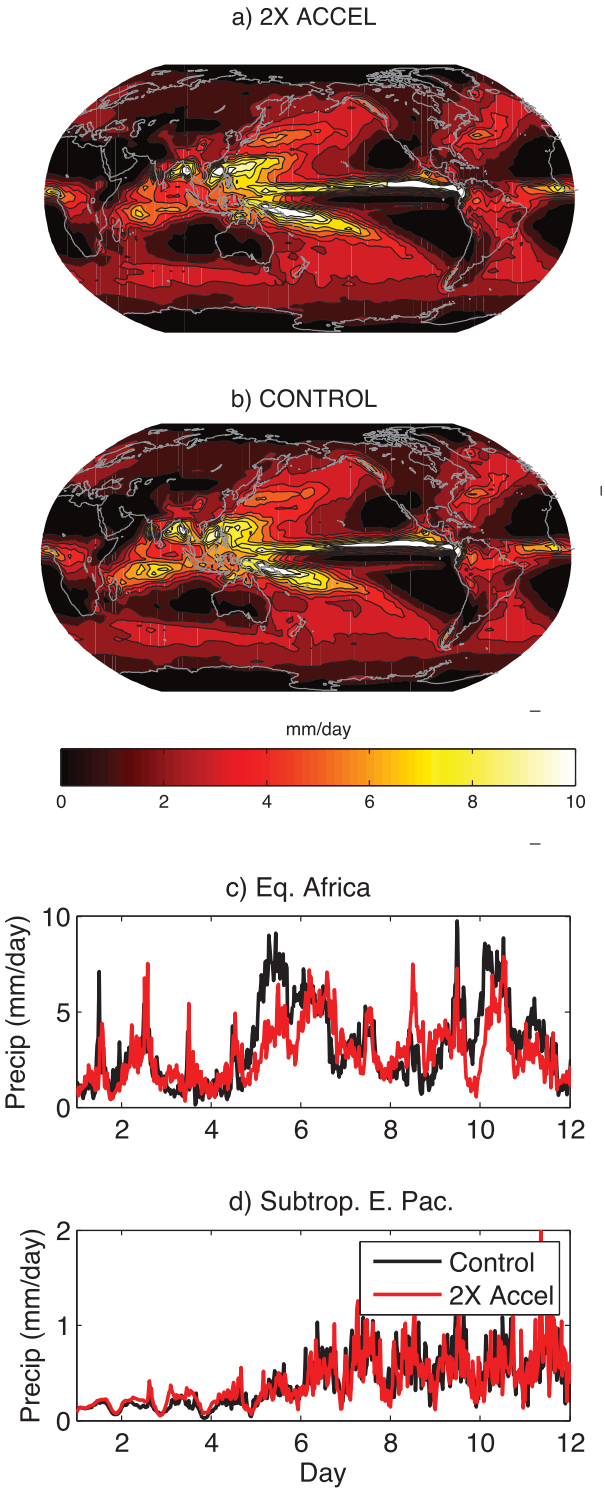

Figure 11. As in Figure 10, but for surface precipitation.

regional time series (bottom) broadly capture the low frequency, diurnal cycle, and high-frequency variations as well. The agreement is particularly impressive in the subtropical East Pacific. The mean-state acceleration induced time shift of surface precipitation, shown most clearly over days 1–4 in Figure 11c, is smaller than in the KWAJEX case. This is expected because the acceleration factor is smaller.

Figure 12 shows a wavenumber-frequency spectrum of equatorially symmetric 10°S–10°N averaged anomalies of outgoing longwave radiation [*Wheeler and Kiladis*, 1999] for the 4 year simulation period, demonstrating similar equatorial wave characteristics between the control and 2X accelerated run, including resilient moist Kelvin wave and Madden-Julian Oscillation dispersion characteristics. Indeed, comparing the two plots of Figure 12 without captions, one would be hard pressed to pick out which is the control and which is the accelerated simulation. These simulation results demonstrate the viability of mean-state acceleration for superparameterization.

7. Time Scales and Accuracy

In section 2, we motivated mean-state acceleration based on scale separation between the mean state and eddy time scales. Quantifying the relationship between the underlying characteristic time scales and the accuracy and stability properties of this technique is an open research problem that is beyond the scope of this study, but a brief exploration based on the case studies is presented here.

We estimate the eddy time scale, τ_e, as a ratio of an eddy length scale, L_e, to a characteristic eddy velocity scale, V_e. Using control simulations from each of the case studies, we measure L_e as the mean height of the deepest cloud, z_t, identified as the highest level for which the cloud fraction exceeds 1%. For the steadily forced BOMEX, DYCOMSII-RF01, and S12 cases, this approximately corresponds to the depth of the boundary layer. L_e estimated this way serves as an upper bound length scale for the largest eddies. We estimate V_e as the mean of $\sqrt{\overline{w'^2}}$ below z_t.

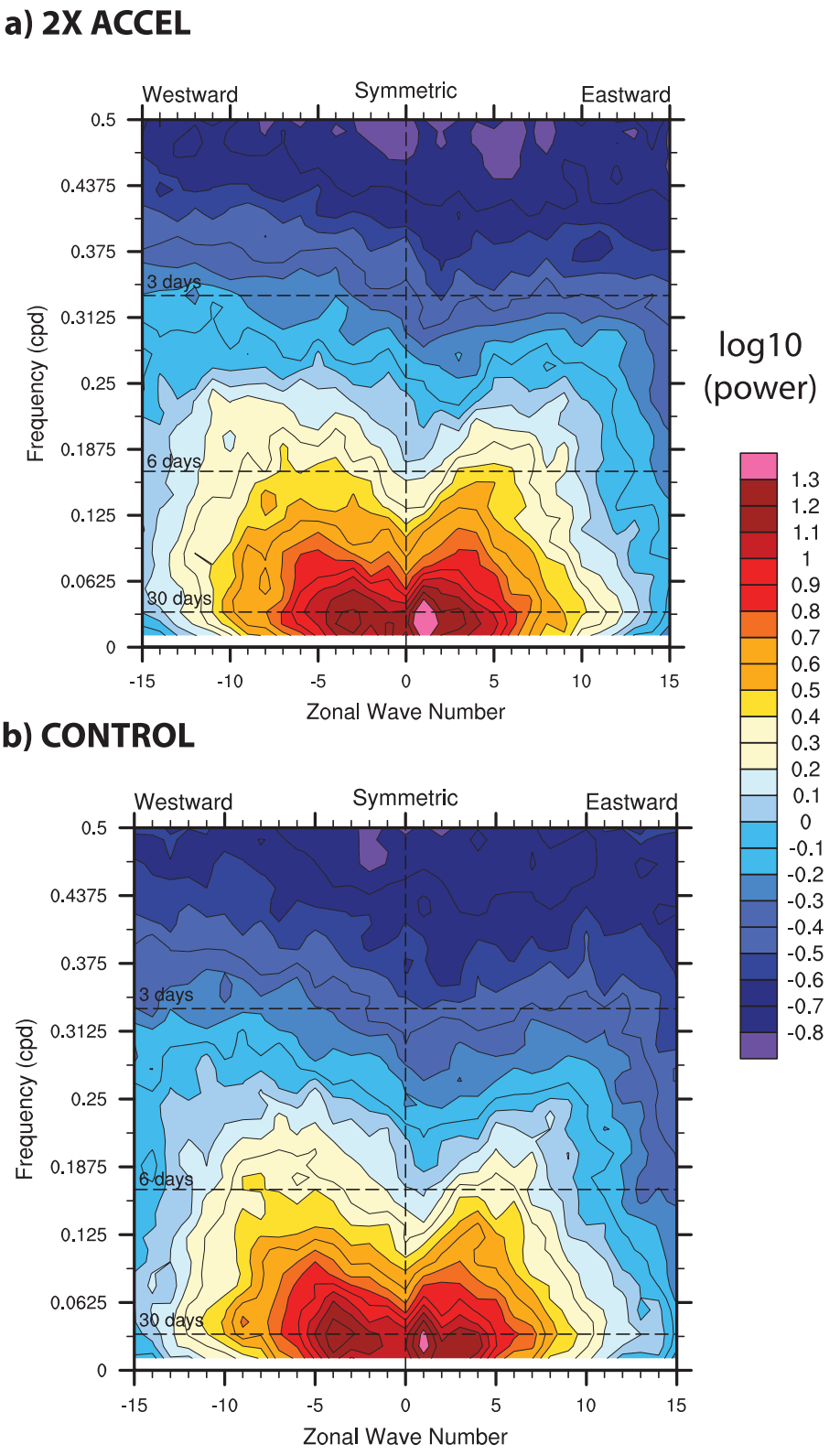

Figure 12. Wheeler-Kiladis diagram showing the equatorially symmetric wave spectrum in 10°S–10°N daily outgoing longwave radiation anomalies from 4 year SPCAM simulations using (top) 2X acceleration versus (bottom) control. Results show the tropical wave spectrum is resilient to acceleration.

Table 1. Time Scale Estimates and Acceleration Accuracy and Stability Thresholds[a]

Case	τ_m (h)	τ_e (h)	τ_m/τ_e	Acc. Thresh.	Stab. Thresh.
BOMEX	750	1.4	560	4	48
DYCOMSII-RF01	190	0.6	330	4	40
KWAJEX	16	7.5	2	6	8
CTL S12	700	0.3	2000	8	32
P2 S12	940	0.3	2700	8	32

[a] τ_m is the mean-state time scale and τ_e the eddy time scale, calculated as discussed in the text. The third column shows their ratio. Column 4 shows the maximum acceleration factor for which the method is accurate throughout the duration of the simulation, and column 5 shows the acceleration factor at which simulations were found to be unstable. Further discussion is presented in the text.

Estimating a single mean-state time scale from the simulations is inherently more uncertain than characterizing the eddy time scale, and it is not entirely clear what the best measure of this time scale is. Thus, we stress that the mean-state scales presented here should be interpreted only as order of magnitude estimates. For the steadily forced cloud-topped boundary layer cases, we use the evolution of the boundary layer depth to estimate the mean-state time scale as

$$\tau_m \approx \frac{\overline{z_t}}{\overline{dz_t/dt}}, \tag{11}$$

where $\overline{z_t}$ is averaged over the first 0.2–1 days of the simulation, and $\overline{dz_t/dt}$ is determined from the slope of a linear least squares fit over the same time frame. This time range is chosen to capture the period after initial model spin-up during which the mean state is evolving most rapidly. Measured in this way, $\tau_m \approx 190$ h for DYCOMSII-RF01, within a factor of 3 of the inversion deepening time scale of 74 h identified by previous mixed-layer model analyses of this case [*Bretherton et al.*, 2010; *Jones et al.*, 2014], suggesting this measure is suitable for an order of magnitude estimate.

For the KWAJEX case, the mean-state evolution is most severely limited by the external forcing time scale, rather than the "internal" time scale of the mean-state response to steady forcings. We crudely estimate the forcing time scale as the first zero of the surface precipitation autocorrelation function.

Eddy and mean-state time scales are presented in Table 1. For each of the shallow cases, the eddy time scale is on the order of 1 h or less. This is substantially shorter than the mean-state time scale (verifying the assumed scale separation). The ratio of $\tau_m/\tau_e \approx O(10^2)$ or higher for these cases.

It is clear from time scale estimates for the KWAJEX case that deep convection represents a fundamentally different challenge for this method, with little time scale separation between the mean-state and turbulent time scales. This is due both to longer eddy length scale and the short forcing time scale. It is not surprising, therefore, that of all cases considered here the acceleration factor is most stringently constrained for deep convection. This furthermore suggests that mean-state acceleration in superparameterization will be similarly constrained, though we have not explored the acceleration limits for SPCAM.

The fourth column of Table 1 shows the highest acceleration factor for which the accelerated simulation was deemed to be accurate, determined by requiring that the difference between the accelerated and control TWP remains within 1.5 standard deviations of the detrended control simulation throughout the entire simulation after allowing for spin-up. This measure of accuracy is more stringent than may be required for a given application. For example, if one is only interested in the steady state solution, accuracy can be achieved with much higher acceleration factors because the error due to accelerating the mean-state damps to zero as the steady state is approached, as demonstrated by the CGILS S12 simulations.

The final column of Table 1 shows the lowest acceleration factor tested for which mean-state acceleration became unstable. For all cases except KWAJEX, the method loses accuracy well before bumping up against the stability ceiling. KWAJEX appears to be stability limited, and somewhat surprisingly the maximum acceleration factor is comparable to our estimate for the ratio of mean state to eddy time scales. For all other cases, both the stability and accuracy thresholds occur for acceleration factors much smaller than the ratio of time scales. Surprisingly, neither the stability threshold nor the accuracy threshold clearly scales with the time scale separation as estimated here. Whether this insensitivity is due to the way the time scales are estimated or due to contributions from other factors not considered here should be the subject of further study, because gaining a clear understanding of which factors limit accuracy and stability may allow us to devise a method to automatically adjust to the ideal acceleration factor during the course of a simulation.

8. Discussion and Conclusions

We have demonstrated that mean-state acceleration is a robust and viable method for speeding up CRM and superparameterized simulations in which the turbulent circulations and clouds evolve faster than the CRM horizontal-mean state. The method was shown to be stable for a range of acceleration factors. While the maximum acceleration factor allowed by stability considerations varied based on the situation, in all cases we achieved from 2X to 8X speedup without seriously degrading the accuracy of the solution.

The accelerated SPCAM tests shown in Figures 10–12 show that 2X mean-state acceleration of the embedded CRMs in a superparameterized model produces realistic climate states and tropical wave spectra at substantial computational savings. Furthermore, this technique is almost trivial to implement in a CRM, and we see little downside to using mean-state acceleration to speedup CRM, LES, and superparameterized simulations.

We have presented the acceleration technique here in its most basic realistic form. Further consideration is needed to apply acceleration to additional prognostic tracers. This approach should generalize to any number of tracers. Following the discussion in section 2, choosing whether or not to accelerate a tracer will depend on whether there is significant storage of the tracer on long time scales, which in turn is related to its source and sink time scales. Similarly, in the case that one wishes to apply mean-state acceleration to precipitation, added care may be needed to ensure that the CFL stability criterion is not violated by the precipitation fall speed. One could separately sub-step the falling precipitation process, though we have not tested this.

For the evolution and mean-state statistics of an accelerated simulation to mimic that of an unaccelerated control simulation, the turbulent eddies must remain tethered to the mean state so that they produce the "correct" contribution to the horizontal-mean tendency. In general, this will not be the case during the model spin-up period, and may be challenged during periods of transient evolution when the state is rapidly changing. Such was the case during the evolution of DYCOMSII-RF01, where acceleration factors $a \geq 8$ suppressed entrainment while the boundary layer was deepening, resulting in overestimated LWP that in turn supported excess boundary layer deepening and delayed the transition to the decoupled steady state.

One important future issue to address is the feasibility of identifying an optimal acceleration factor based on desired accuracy requirements and characteristic time scales that can be estimated a priori or as the simulation evolves. Doing so could provide a way to automatically adjust the acceleration factor throughout the course of a simulation and would obviate the need to benchmark accelerated simulations against an unaccelerated run to verify their accuracy.

Although we have focused on using $a > 1$ to accelerate simulations, it may at times be advantageous to use $a < 1$, such as during model spin-up to allow the turbulent eddies to develop while constraining the mean state from drifting from the initial state.

Overall, the mean-state acceleration scheme's success across a broad class of models (CRM, LES, and superparameterization) can benefit diverse lines of atmospheric science research that involve long integrations of such models that are currently computationally constrained. Examples include cloud feedback studies such as our CGILS case, large-domain simulations of deep and boundary layer convection, and multidecadal ocean-coupled superparameterized climate simulation.

Appendix A: Mean-State Acceleration as Seamless HMM

An alternative way to motivate mean-state acceleration which provides added insight into the approach and its formal grounding is to interpret it as a seamless heterogeneous multiscale method (HMM) [*Abdulle et al.*, 2012, and references therein]. Consider a scale-separated system consisting of a microscale state (μ) and macroscale state (M). The macrostate is evolved according to

$$M(T+\Delta T) = S_{\Delta T}(M(T); D(T)), \tag{A1}$$

where S is the macroscale evolution operator, ΔT the native time step of the macromodel, and D represents data that must be supplied from the microscale state. Similarly, the microstate is evolved according to a microscale model,

$$\mu(t+\Delta t) = \mathcal{S}_{\Delta t}(\mu(t); M(t)), \tag{A2}$$

where $\mathcal{S}$ is the microscale evolution operator and Δt the native time step of the micromodel.

The seamless HMM algorithm evolves the microstates and macrostates with different clock speeds while exchanging data at regular intervals according to the following steps [*Abdulle et al.*, 2012]:

1. Given the current state of the microstate $\mu(t)$ and macrostate $M(T)$, evolve the micromodel for one time step:
$$\mu(t+\Delta t) = \mathcal{S}_{\Delta t}(\mu(t); M(T)).$$
2. Estimate D from the microstate.
3. Evolve the macrostate by
$$M(T+\Delta T) = S_{\Delta T}(M(T); D),$$

and begin the next iteration with microstate $\mu(t+\Delta t)$ and $M(T+\Delta T)$.

A conventional HMM reconstructs and reinitializes μ at each time step from the macro-state, and then the micromodel runs for several time steps to reach a quasi-equilibrium. By contrast, the seamless approach requires no reinitialization, but instead exchanges data between the models at each time step. The trade-off is that the micromodel must have sufficient time to relax to the changing macrostate, limiting the size of ΔT.

In the context of (1)–(3), we identify $\mu = \phi'$, $M = \bar{\phi}$, Δt as the native CRM time step, $\Delta T = a\Delta t$, $\mathcal{S}_{\Delta t}$ is the evolution operator corresponding to f' in (3), and $S_{\Delta T}$ the evolution operator corresponding to $\bar{f}$ in (2). The data D required by the macromodel is implicitly used in the horizontal averaging step which calculates $\bar{f}$, since this includes horizontally averaged turbulence source terms. Indeed, the simplicity of the macromodel in this case allows us to seamlessly apply the macrostate acceleration entirely within the framework of the original CRM, as in section 3.

Acknowledgments
The authors acknowledge support from NOAA MAPP grant GC13-560 as a part of the NOAA Cloud and Boundary-Layer Process Climate Process Team, and by the U.S. Department of Energy under DE-SC0012152, DE-SC0012451, and DE-SC0012548. The SAM LES is maintained by Marat Khairoutdinov, and is available at http://rossby.msrc.sunysb.edu/~marat/SAM.html. The input files and source code modifications necessary to reproduce the results presented in Section 5 are available at http://atmos.uw.edu/~cjones/sam_accel/. Specific modifications of SPCAM3 code corresponding to the version of CRM mean-state acceleration reported in this paper are preserved at revision 365 of the SPCAM3.0 code branch maintained by the Center for Multiscale Modeling of Atmospheric Processes at https://svn.sdsc.edu/repo/cmmap/cam3_sp/branches/pritchard.

References

Abdulle, A., E. Weinan, B. Engquist, and E. Vanden-Eijnden (2012), The heterogeneous multiscale method, *Acta Numer.*, *21*, 1–87, doi:10.1017/S0962492912000025.

Blossey, P. N., and D. R. Durran (2008), Selective monotonicity preservation in scalar advection, *J. Comput. Phys.*, *227*(10), 5160–5183, doi:10.1016/j.jcp.2008.01.043.

Blossey, P. N., C. S. Bretherton, J. Cetrone, and M. Kharoutdinov (2007), Cloud-resolving model simulations of KWAJEX: Model sensitivities and comparisons with satellite and radar observations, *J. Atmos. Sci.*, *64*, 1488–1508.

Blossey, P. N., C. S. Bretherton, M. Zhang, A. Cheng, S. Endo, T. Heus, Y. Liu, A. P. Lock, S. R. de Roode, and K.-M. Xu (2013), Marine low cloud sensitivity to an idealized climate change: The CGILS LES intercomparison, *J. Adv. Model. Earth Syst.*, *5*, 234–258, doi:10.1002/jame.20025.

Bretherton, C. S., J. Uchida, and P. N. Blossey (2010), Slow manifolds and multiple equilibria in stratocumulus-capped boundary layers, *J. Adv. Model. Earth Syst.*, *2*, 14, doi:10.3894/JAMES.2010.2.14.

Bretherton, C. S., P. N. Blossey, and C. R. Jones (2013), Mechanisms of marine low cloud sensitivity to idealized climate perturbations: A single-LES exploration extending the CGILS cases, *J. Adv. Model. Earth Syst.*, *5*, 316–337, doi:10.1002/jame.20019.

Bryan, K. (1984), Accelerating the convergence to equilibrium of ocean–climate models, *J. Phys. Oceanogr.*, *14*, 666–673.

Chorin, A. J. (1967), A numerical method for solving incompressible viscous flow problems, *J. Comput. Phys.*, *2*(1), 12–26.

Grabowski, W. (2001), Coupling cloud processes with the large-scale dynamics using the cloud-resolving convection parameterization (CRCP). *J. Atmos. Sci.*, *58*, 978–997.

Holland, J. Z., and E. M. Rasmusson (1793), Measurements of atmospheric mass, energy, and momentum budgets over a 500-kilometer square of tropical ocean, *Mon. Weather Rev.*, *101*, 44–55, doi:10.1175/1520-0493(1973)101<0044:MOTAME>2.3.CO;2.

Jones, C. R., C. S. Bretherton, and P. N. Blossey (2014), Fast stratocumulus time scale in mixed layer model and large eddy simulation, *J. Adv. Model. Earth Syst.*, *6*, 206–222, doi:10.1002/2013MS000289.

Khairoutdinov, M., and Y. Kogan (2000), A new cloud physics parameterization in a large-eddy simulation model of marine stratocumulus, *Mon. Weather Rev.*, *128*(1), 229–243.

Khairoutdinov, M. F., and D. A. Randall (2001), A cloud-resolving model as a cloud parameterization in the NCAR Community Climate System Model: Preliminary results, *Geophys. Res. Lett.*, *28*, 3617–3620, doi:10.1029/2001GL013552.

Khairoutdinov, M. F., and D. A. Randall (2003), Cloud resolving modeling of the ARM summer 1997 IOP: Model formulation, results, uncertainties, and sensitivities, *J. Atmos. Sci.*, *60*(4), 607–625, doi:10.1175/1520-0469(2003)060<0607:CRMOTA>2.0.CO;2.

Khairoutdinov, M., D. Randall, and C. DeMott (2005), Simulations of the atmospheric general circulation using a cloud-resolving model as a superparameterization of physical processes, *J. Atmos. Sci.*, *62*, 2136–2154, doi:10.1175/JAS3453.1.

Kuang, Z., P. N. Blossey, and C. S. Bretherton (2005), A new approach for 3D cloud resolving simulations of large scale atmospheric circulation, *Geophys. Res. Lett.*, *32*, L02809, doi:10.1029/2004GL021024.

Liu, Z., W. Lewis, and A. Ganopolski (2004), An acceleration scheme for the simulation of long term climate evolution, *Clim. Dyn.*, *22*, 771–781.

Miyamoto, Y., Y. Kajikawa, R. Yoshida, T. Yamaura, H. Yashiro, and H. Tomita (2013), Deep moist atmospheric convection in a subkilometer global simulation, *Geophys. Res. Lett.*, *40*, 4922–4926, doi:10.1002/grl.50944.

Mlawer, E., S. Taubman, P. Brown, M. Iacono, and S. Clough (1997), Radiative transfer for inhomogeneous atmospheres: RRTM, a validated correlated-k model for the longwave, *J. Geophys. Res.*, *102*(D14), 16,663–16,682, doi:10.1029/97JD00237.

Pauluis, O., D. Frierson, S. T. Garner, I. M. Held, and G. K. Vallis (2006), The hypohydrostatic rescaling and its impacts on modeling of atmospheric convection, *Theor. Comput. Fluid Dyn.*, *20*, 485–489, doi:10.1007/s00162-006-0026-x.

Pritchard, M. S., C. S. Bretherton, and C. A. DeMott (2014), Restricting 32–128 km horizontal scales hardly affects the MJO in the Superparameterized Community Atmosphere Model v.3.0 but the number of cloud-resolving grid columns constrains vertical mixing, *J. Adv. Model. Earth Syst.*, *6*, 723–739, doi:10.1002/2014MS000340.

Siebesma, A. P., et al. (2003), A large-eddy simulation intercomparison study of shallow cumulus convection, *J. Atmos. Sci.*, *60*, 1201–1219.

Slawinska, J., O. Pauluis, A. J. Majda, and W. W. Grabowski (2015), Multiscale interactions in an idealized Walker cell: Simulations with sparse space–time superparameterization, *Mon. Weather Rev.*, *143*, 563–580, doi:10.1175/MWR-D-14-00082.1.

Stevens, B., and D. H. Lenschow (2001), Observations, experiments, and large eddy simulation, *Bull. Am. Meteorol. Soc.*, *82*, 283–284.

Stevens, B., et al. (2003), Dynamics and chemistry of marine stratocumulus—DYCOMS-II, *Bull. Am. Meteorol. Soc.*, *84*, 579–593.

Stevens, B., et al. (2005), Evaluation of large-eddy simulations via observations of nocturnal marine stratocumulus, *Mon. Weather Rev.*, *133*, 1443–1462.

Tomita, H., H. Miura, S. Iga, T. Nasumo, and M. Satoh (2005), A global cloud-resolving simulation: Preliminary results from an aquaplanet experiment, *Geophys. Res. Lett.*, *32*, L08805, doi:10.1029/2005GL022459.

Wheeler, M., and G. N. Kiladis (1999), Convectively coupled equatorial waves: Analysis of clouds and temperature in the wavenumber-frequency domain, *J. Atmos. Sci.*, *56*, 374–399.

Xing, Y., A. J. Majda, and W. W. Grabowski (2009), New efficient sparse space-time algorithms for superparameterization on mesoscales, *Mon. Weather Rev.*, *137*, 4307–4324, doi:10.1175/2009MWR2858.1.

Zhang, M., et al. (2013), CGILS: Results from the first phase of an international project to understand the physical mechanisms of low cloud feedbacks in single column models, *J. Adv. Model. Earth Sys.*, *5*, 826–842, doi:10.1002/2013MS000246.

Zhu, P., et al. (2005), Intercomparison and interpretation of single-column model simulations of a nocturnal stratocumulus-topped marine boundary layer, *Mon. Weather Rev.*, *133*(9), 2741–2758.